Measured and Modeled Radiation Profiles for LHD Plasma – A Comparison during Plasma Detachment*)

Shwetang N. PANDYA[1)], Byron J. PETERSON[2)], Masahiro KOBAYASHI[2)], Kiyofumi MUKAI[2)], Ryuichi SANO[1)], Hirohiko TANAKA[2)], Suguru MASUZAKI[2)] and LHD Experiment Group

[1)]*The Graduate University for Advance Studies, 322-6 Oroshi-cho, Toki 509-5292, Japan*
[2)]*National Institute for Fusion Science, 322-6 Oroshi-cho, Toki 509-5292, Japan*

(Received 26 November 2013 / Accepted 29 March 2014)

Detached (from the divertors) plasma regime is a very important operational phase for future fusion device operation and is sustained in the Large Helical Device (LHD) by applying an $m/n = 1/1$ resonant magnetic perturbation (RMP). The radiation from the plasma is found to be localized near the X-point of this RMP during plasma detachment which is confirmed both by the EMC3-EIRENE edge impurity transport code and experiments. This agreement motivates the establishment of a comparison between the results from the transport model and InfraRed imaging Video Bolometer (IRVB) experiments. A synthetic instrument has been developed which can simulate the radiation by tracing the sight lines through the three dimensional carbon impurity radiation results of the EMC3-EIRENE, giving a synthetic image. These synthetic images can be compared with the IRVB image obtained experimentally. Such a comparison is attempted here for two IRVBs installed on LHD for the data from the 2012 and 2013 experimental campaigns. The comparison reveals a fair amount of qualitative agreement but quantitative disagreement among both the approaches. Probable causes for the disagreement are discussed and corrective measures are suggested.

© *2014 The Japan Society of Plasma Science and Nuclear Fusion Research*

Keywords: IRVB, plasma detachment, radiation localization, resonant magnetic perturbation, synthetic diagnostic, edge transport model EMC3-EIRENE

DOI: 10.1585/pfr.9.3402064

1. Introduction

Heat load reduction on the plasma facing components (PFCs) is one of the key research issues for future, reactor grade plasma confinement devices and draws a lot of concern since the lifetime and the integrity of the PFCs rely on techniques that can substantially reduce the heat loads reaching the PFCs, well within their design limits. Currently, several methods are tried on many plasma confinement devices around the globe to ensure that the heat loads get partially dissipated before reaching the PFCs. The detached plasma regime, also termed the radiative divertor regime, is seen as a strong candidate for the dissipation of heat flux through impurity radiation. Sustaining the detached plasma regime in a tokamak offers several challenges since the radiative zone initiated in front of the divertor gradually moves upstream towards the magnetic null (divertor X-point), resulting in the formation of a MARFE, which often penetrates into the plasma core leading to thermal instabilities and the termination of the plasma. The LHD has experimentally demonstrated that divertor detachment can be achieved and sustained by the addition of an externally induced $m/n = 1/1$ resonant magnetic perturbation (RMP). The RMP is introduced into the stochastic boundary of the LHD plasma by energizing 10 pairs of saddle perturbation coils installed at the top and bottom ports of every LHD field period. Addition of the RMP seems to favor the detached plasma regime by localizing the radiating region near the RMP X-point, restricting its movement and penetration into the core, hence avoiding plasma termination by radiative collapse. The localized radiation during the plasma detachment can be effectively studied experimentally [1–3] by the InfraRed imaging Video Bolometer (IRVB) [4]. This localization is also confirmed by the EMC3-EIRENE [5, 6] edge impurity transport code. This agreement motivates the establishment of a comparison between the results from the transport model and experiments. The comparison is not intended to establish any sort of exact quantitative agreement; but to identify the extent to which the modeling can reproduce the experimental data. Such a comparison can be regarded as a first step for improving the assumptions considered for the transport model. This paper focuses on the comparison between the modeling predictions from the edge transport code and IRVB results obtained during plasma detachment experiments on LHD. Section 2 describes the principle and data analysis method for the IRVB. Section 3 gives an explanation about the generation of synthetic images by using a synthetic instrument. Discharge parameters are explained in Section 4. Results from the upper port and the tangential

author's e-mail: pandya.shwetang@LHD.nifs.ac.jp
*) This article is based on the presentation at the 23rd International Toki Conference (ITC23).

© 2014 The Japan Society of Plasma Science and Nuclear Fusion Research

port IRVB are compared with corresponding synthetic images and discussed in Sections 5 and 6 respectively. Conclusions are given in Section 7.

2. Infrared Imaging Video Bolometer (IRVB)

The InfraRed imaging Video Bolometer (IRVB) is an inevitable diagnostic for studying two dimensional (2D) radiation patterns from the three dimensional (3D) LHD plasma. The IRVB has been developed in part to meet the challenging demands of the 3D physics of a helical device through the large number of channels and imaging capabilities afforded by this diagnostic. IRVBs are successfully diagnosing the LHD plasmas for more than a decade and currently four IRVBs are operational for studying the 3D edge physics of LHD. IRVBs are used to study the localization of radiation structures near the $m/n = 1/1$ resonant magnetic perturbation (RMP) X-points during plasma detachment and also for 3D tomography on LHD. The IRVB is based on the simple principle of a pinhole camera where the radiation from the plasma is collimated onto the 2.5 μm thin platinum foil mounted in a frame acting as a radiation absorber. This pinhole geometry insures that each pixel of the IRVB foil has a unique line of sight. The IRVB foil is blackened on both sides by an aerosol-based graphite spray to increase the emissivity. The absorbed radiation from the plasma raises the temperature of the foil which is measured by an infrared camera placed on the other side of the foil, outside the LHD vacuum vessel in a soft iron magnetic shield box. Figure 1 illustrates the IRVB concept by a CAD layout.

The radiated power from the plasma falling on the foil can be estimated by numerically solving the 2D heat diffusion Eq. (1) using the spatiotemporal variation in the foil temperature obtained from the infrared camera.

$$S_{\mathrm{rad}} = S_{\mathrm{bb}} + \frac{1}{\kappa}\frac{\partial T}{\partial t} - \left[\frac{\partial^2 T}{\partial x^2} + \frac{\partial^2 T}{\partial y^2}\right]. \quad (1)$$

Where $S_{\mathrm{bb}} = \varepsilon\sigma_{\mathrm{SB}}(T^4 - T_0^4)/kt_{\mathrm{f}}$ is blackbody cooling term and $S_{\mathrm{rad}} = P_{\mathrm{incident}}/kt_{\mathrm{f}}l^2$ is the radiation density on the foil. In Eq. (1) P_{incident} is the power incident on the foil, T is the measured temperature, while k, t_{f} and κ are the thermal conductivity, thickness and thermal diffusivity of the foil, respectively. l^2 is the area of IRVB pixel, σ_{SB} is the Stephen-Boltzmann constant and ε is the emissivity of the graphite coating used on the foil. The thermal (k, κ), physical (t_{f}) and optical (ε) properties of the foil are determined separately by dedicated foil calibration experiments. The 2D power density profiles obtained by such an analysis can now be compared with the modeling results from the synthetic instrument.

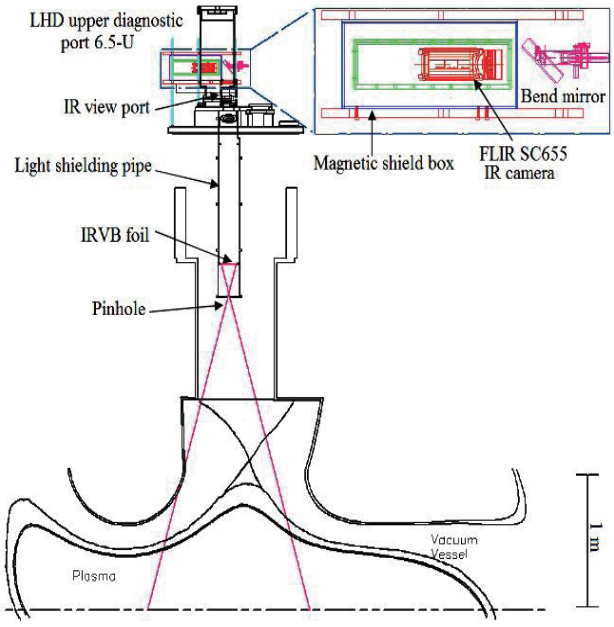

Fig. 1 CAD cartoon of upper port IRVB on LHD.

3. Synthetic Instrument

Figure 2 (a) shows the estimated edge radiation from EMC3-EIRENE for a magnetic configuration without an RMP, for one poloidal cross-section. Only atomic carbon is considered for the impurity transport modeling with an ejection energy of 0.05 eV assuming dominant chemical sputtering, both from the divertor and walls, with a sputtering coefficient of 1%. This assumption is valid since physical sputtering yields are an order of magnitude less as compared to the chemical sputtering yields [7]. The reason for considering only atomic carbon is well justified since no significant radiation from the high Z impurities like Fe has been observed experimentally [8]. The fraction of radiation from the edge region computed for the amount of Fe reported in Ref. 8 is about 3.6% of the total input power which is much less than the radiation from atomic carbon. There is also enough experimental evidence about the negligible concentration of hydrocarbon impurities. The figure reveals that the radiation is mostly localized at the helical divertor X-points (HDX). Figure 2 (b) shows the EMC3-EIRENE estimation for the RMP assisted detachment magnetic configuration, which clearly shows the localization of the radiation near the magnetic island X-point (MIX). A synthetic instrument uses a code that can trace the sight-lines for all the detectors of the IRVB through the 3D radiation intensity distribution given by EMC3-EIRENE. The synthetic instrument then integrates the radiation for each sight line of the IRVB, considering the pinhole and machine geometry, which results in a 2D distribution of the power density from the plasma at the IRVB foil. This 2D distribution of power densities obtained from the synthetic instrument is called a synthetic image. The synthetic instrument utilizes two matrices to estimate the power falling on the IRVB detector. The emissivity matrix, S_j, is the 3D distribution of radiation obtained from EMC3-EIRENE edge transport modeling. Since the output from EMC3-EIRENE is irregularly spaced and with a much finer spatial

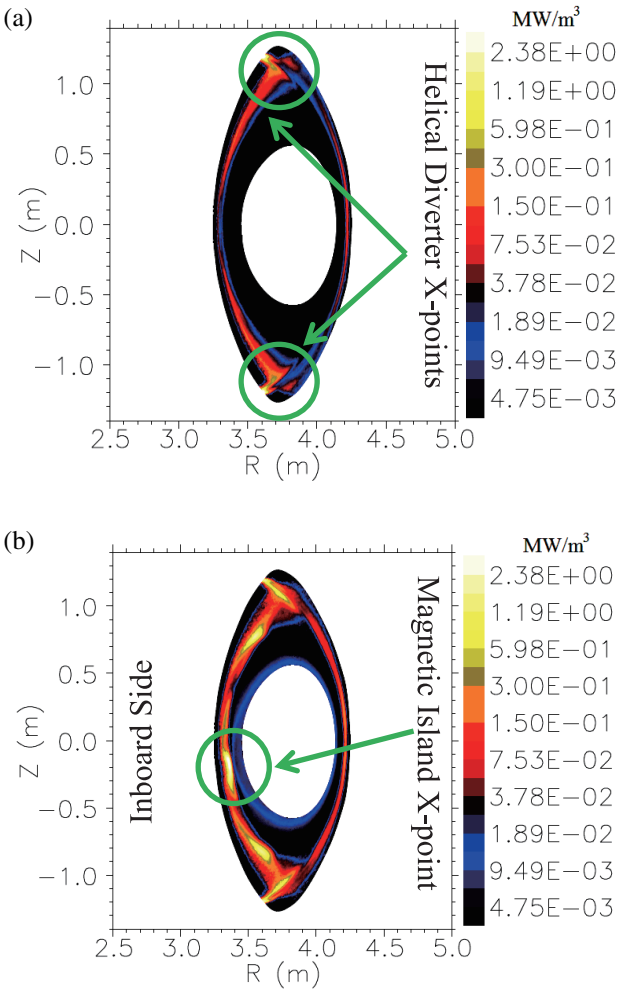

Fig. 2 (a) Poloidal radiation distribution estimated by EMC3-EIRENE without RMP (attached). (b) Poloidal radiation distribution estimated by EMC3-EIRENE with RMP (during detachment).

resolution, S_j is obtained by regularizing and re-sampling the EMC3-EIRENE data into a course grid with radial and azimuth spatial resolutions of 5 cm each and a toroidal resolution of 1° using an interpolation technique. The geometry matrix, T_{ij} is calculated by multiplying the detector solid angle Ω_{ij} (resulting from the IRVB pixel area and its distance from the sub-voxel) and the intersection volume V_{ij}, (resulting from the intersection of the bolometer chord volume and the plasma volume). The power falling on the IRVB detector can be estimated by multiplying both these matrices as shown in Eq. (2).

$$P_i = \sum_j \frac{\Omega_{ij}}{4\pi} V_{ij} S_j = \sum_j T_{ij} S_j. \quad (2)$$

Such a synthetic image can be compared with the power density distribution obtained experimentally by the IRVB. Such a comparison is attempted in the following sections for two different IRVBs installed at tangential and upper ports of LHD.

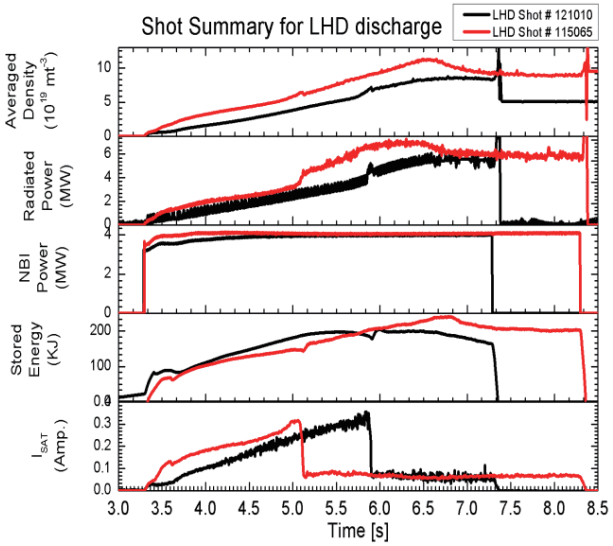

Fig. 3 Detached Plasma Parameters for LHD Discharge.

4. Plasma Discharge Parameters

LHD discharges # 115065 and # 121010 with an RMP applied at the 6th port is considered for this paper. The vacuum magnetic axis R_{ax} is located at 3.9 m and the average minor radius is around 0.7 m. Three negative beam NBIs with a nominal acceleration voltage of 180 keV are used to heat the plasma. The saddle perturbation coils are charged with 3.4 kA current prior to the discharge so as to establish an RMP at the 6th port. The density is gradually ramped up, with a constant NBI power, till the plasma detaches from the divertors as shown in Fig. 3. The detachment can be clearly visualized from the ion saturation current (I_{SAT}) graph showing an abrupt decrease in I_{SAT} measured by the divertor probes located on the inboard side near the 7th port. Detachment can also be inferred from a slight increase in the radiated power and plasma stored energy (after a brief negative spike) at the time of detachment. The detachment seems to be stably sustained till the discharge terminates by the shutdown of the NBI beam.

5. Modeling and Experiment – A Comparison for the Upper Port IRVB

The upper port IRVB views a vertically elongated plasma column of LHD as shown in Fig. 1. A platinum foil of dimensions $130 \times 100\,\mathrm{mm}^2$, held in a copper frame is used as a radiation absorber. The dimensions of the pinhole are $8 \times 8\,\mathrm{mm}^2$. The temperature rise of the foil is monitored by a FLIR SC655 infrared camera working in the $7.5 \sim 12\,\mu\mathrm{m}$ wavelength range having a 640×480 pixel microbolometer focal plane array (FPA). The camera sensitivity is 50 m°K with a field of view (FoV) of $15° \times 11°$ and operates at 50 fps in full frame mode. The noise equivalent power density of this IRVB is $145\,\mu\mathrm{W/cm}^2$. The thermal images acquired by the IR camera are trimmed so as to

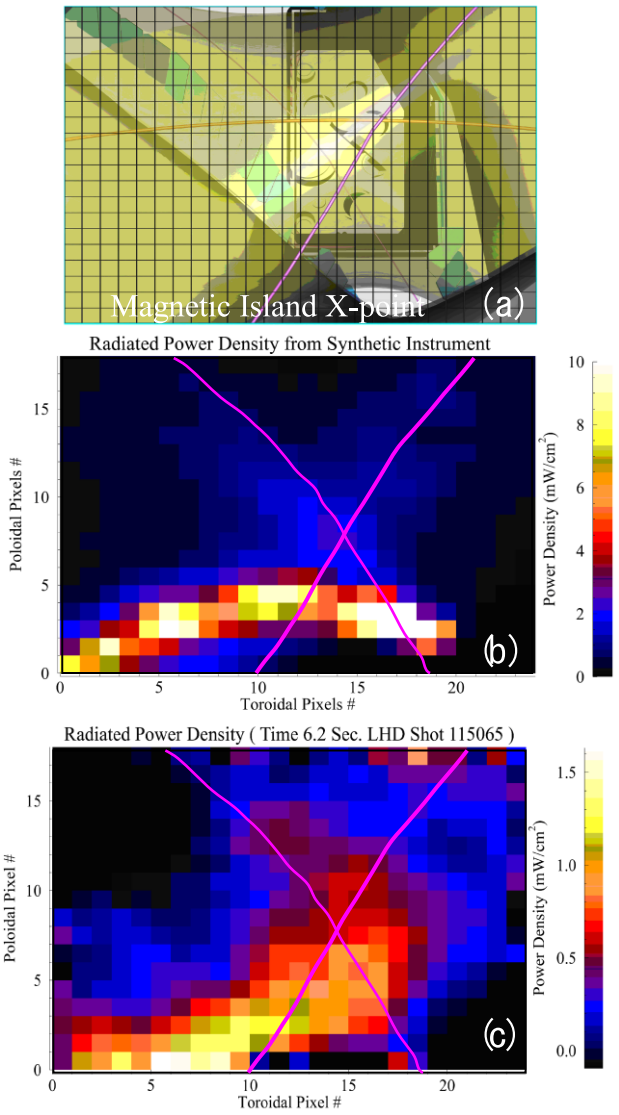

Fig. 4 (a) CAD FoV traced from the foil location through the pinhole. The CAD shows IRVB pixels (grid), magnetic axis (curved yellow line), approximate location for the upper and lower helical divertor X-points (thick and thin pink lines respectively). (b) Synthetic image during detachment for upstream plasma density $n_{up} = 6.5 \times 10^{19}\,m^{-3}$. (c) Experimental IRVB image during detachment for line averaged plasma density $\langle n_e \rangle = 8.0 \times 10^{19}\,m^{-3}$.

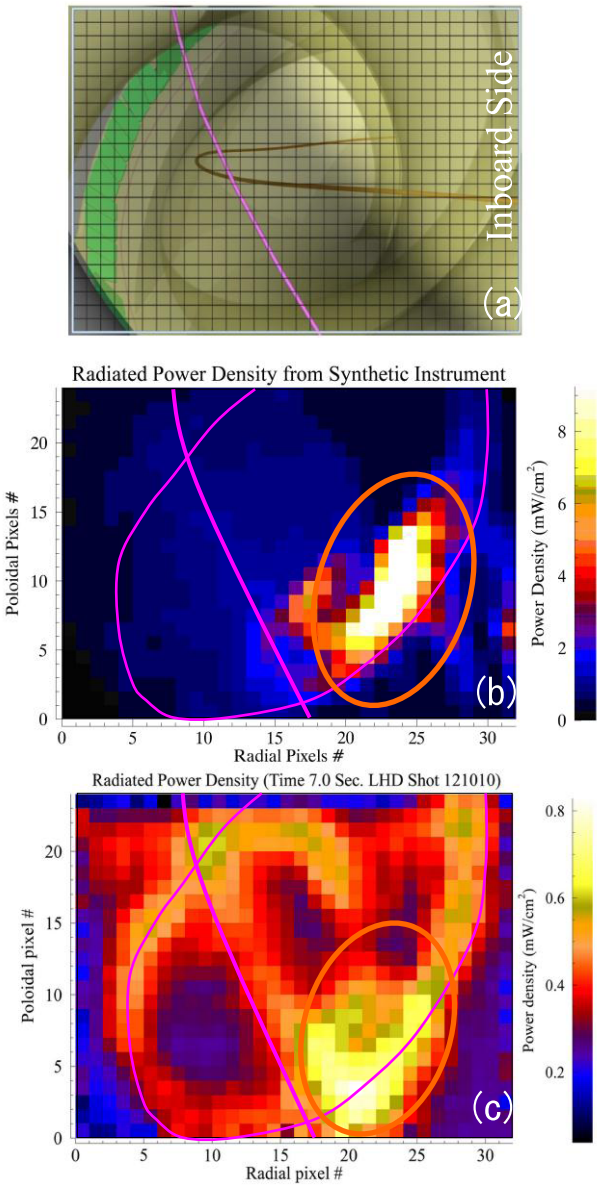

Fig. 5 (a) CAD FoV traced from the foil location through the pinhole. The CAD shows IRVB pixels (grid), magnetic axis (curved brown line), approximate location of the helical divertor X-points (thick and thin pink lines). (b) Synthetic image during detachment for upstream plasma density $n_{up} = 6.5 \times 10^{19}\,m^{-3}$. (c) Experimental IRVB image during detachment for line averaged plasma density $\langle n_e \rangle = 8 \times 10^{19}\,m^{-3}$.

view the foil and re-sampled to 24×18 IRVB pixels so that each IRVB pixel is a linear interpolation over 64 IR camera pixels. This improves the SNR of the diagnostic by 8 times since the noise decreases as the square-root of number of IR camera pixels being averaged over. Figure 4 (a) shows the CAD FoV as traced from the foil location. Figure 4 (b) shows the synthetic image showing the localized radiation following the MIX and Fig. 4 (c) shows the experiment data for the LHD discharge # 115065 from the upper port IRVB, also showing a localization of radiation near the MIX and HDX.

6. Modeling and Experiment – A Comparison for the Tangential Port IRVB

The tangential port IRVB diagnoses the plasma column of LHD with a platinum foil of dimensions $90 \times 70\,mm^2$. The dimensions of the pinhole are $4 \times 4\,mm^2$. A FLIR SC4000 infrared camera working in the 3 - 5 μm wavelength range having a 320×240 pixel sterling cooled FPA is used for foil temperature measurement. The camera sensitivity is 20 m°K with a FoV of $5.5° \times 4.4°$ and op-

erates at 100 fps in full frame mode. The noise equivalent power density of this IRVB is 30 μW/cm^2. The thermal images acquired by the IR camera are re-sampled to 32×24 IRVB pixels so that each IRVB pixel is a linear interpolation over 94 IR camera pixels which improves the SNR of the diagnostic by 9.5 times. Figure 5 (a) shows the CAD FoV as traced from the foil location. Figure 5 (b) shows the synthetic image from the synthetic instrument which shows localized radiation towards the inboard side and Fig. 5 (c) shows the experimental data for the LHD discharge # 121010 from the tangential port IRVB showing a signature of radiation localization near the MIX location towards the inboard side of the torus. Before the detachment the radiation band follows the HDX but soon after the detachment the radiation shifts to follow the MIX indicated by an orange oval. The radiation from the MIX is evident in the experimental image, but much more distinct in the synthetic image. This can be attributed to the overestimation of the radiation in the MIX by the modeling code. A much better correlation is expected once the corrective measures, as mentioned in the next section, are implemented in the model.

7. Conclusion

This paper illustrates the usefulness of the IRVB in exploring the physics of plasma radiation, especially in a 3D machine geometry like LHD. The development of a synthetic instrument and its usefulness for generating the synthetic images, comparable with the experimental data has been demonstrated. A fair amount of qualitative agreement between the modeling and experiment is shown by Figs. 4 and 5. Quantitatively the modeling images predict power densities that are ~ 7 times higher at the locations where the radiation peaks and ~ 2 times higher on an average than its experimental counterpart. Considering hydrocarbons (such as CH_4) in the model, however, might alter the situations to a certain extent through change in the carbon injection energy and also its sputtering coefficient. These processes will then modify the penetration length of carbon impurity into the plasma as well as the amount of impurity which, eventually, will result in modification of the radiation intensity as well as the detachment transition density. Considering only atomic carbon can be one of the reasons for the discrepancy in radiation intensity between experiments and modeling. Investigation of the effects of such molecular impurities, scanning cross-field and impurity transport coefficients in the EMC3-EIRENE code and considering the effects of spatial and temporal averaging in experimental data analysis is left for future work to achieve a better convergence between the experiments and modeling results.

Acknowledgements

This work was supported by NIFS budget codes NIFS13ULHH026 and NIFS13GGHH001.

[1] B.J. Peterson *et al.*, J. Nucl. Mater. **415**, S1147 (2011).
[2] E.A. Drapiko *et al.*, Nucl. Fusion **51**, 073005 (2011).
[3] M. Kobayashi *et al.*, Nucl. Fusion **53**, 093032 (2013).
[4] B.J. Peterson, Rev. Sci. Instrum. **71**, 3696 (2000).
[5] Y. Feng *et al.*, Contrib. Plasma Phys. **44**, 57 (2004).
[6] D. Reiter *et al.*, Fusion Sci. Technol. **47**, 172 (2005).
[7] M. Kobayashi *et al.*, Proc. 22nd Fusion Energy Conf., Geneva, October 13-18, 2008, EX09-4, International Atomic Energy Agency (2008); http://www-pub.iaea.org/MTCD/Meetings/fec2008pp.asp.
[8] S. Morita *et al.*, Nucl. Fusion **53**, 093017 (2013).